ACS APPLIED MATERIALS & INTERFACES

Research Article

www.acsami.org

Two-Step Reset in the Resistance Switching of the Al/TiO_x/Cu Structure

Xing L. Shao,[†] Jin S. Zhao,*[,†] Kai L. Zhang,[†] Ran Chen,[†] Kuo Sun,[†] Chang J. Chen,[†] Kai Liu,[†] Li W. Zhou,[†] Jian Y. Wang,[†] Chen M. Ma,[†] Kyung J. Yoon,[‡] and Cheol S. Hwang*[,†,‡]

[†]School of Electronics Information Engineering, Tianjin Key Laboratory of Film Electronic & Communication Devices, Tianjin University of Technology, Tianjin 300384, China

[‡]WCU Hybrid Materials Program, Department of Materials Science and Engineering, and Inter-university Semiconductor Research Center, Seoul National University, 599 Gwanak-ro, Gwanak-gu, Seoul 151-744, Republic of Korea

ABSTRACT: Two-step reset behaviors in the resistance switching properties of the top Al/TiO_x/bottom Cu structure were studied. During the electroforming and set steps, two types of conducting filaments composed of Cu and oxygen vacancies (Cu-CF and V_O-CF) were simultaneously (or sequentially) formed when Al was negatively biased. In the subsequent reset step with the opposite bias polarity, the Cu-CFs ruptured first at ~0.5 V, and formed an intermediate state. The trap-filled V_O-CFs were transformed into a trap-empty state, resulting in a high-resistance state at ~1 V. Matrix phase in the electrochemical metallization cell can play an active role in resistance switching.

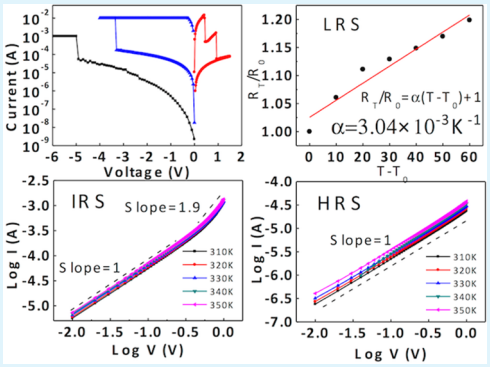

KEYWORDS: *RRAM, multilevel RS, Cu-CF, V_O-CF, TiO_x*

1. INTRODUCTION

Electronic resistance switching (RS) in many oxide and nonoxide materials attracts much attention for the next-generation nonvolatile random access memory[1−4] and other applications, such as neuromorphic computing.[5] Although the RS material systems can be classified into several groups according to the detailed switching mechanisms,[2] this study focuses on the simultaneous presence of two distinctive mechanisms and their combined effects on the RS performance in the Al/TiO_x/Cu RS system, where Al and Cu are the top and bottom electrodes, respectively. As Cu is well-known to be an active metal in the electrochemical metallization memory (ECM),[2,6−8] adopting Cu as the bottom electrode (BE) has a high probability of inducing Cu conducting filament (CF) formation in the TiO_x insulating layer. Meanwhile, adopting Al as the top electrode (TE) on top of TiO_x may induce the oxygen vacancy (V_O) related RS mechanisms such as the Magnéli-phase (Ti_nO_{2n-1}; n = 3, 4, 5...) CF formation,[9,10] or electronic switching related with the trapping and detrapping of carriers along the V_O channels,[11,12] because of the higher oxidation potential of Al compared with Ti.[13] ECM is generally characterized by the inherently bipolar-type RS, whose switching voltages are usually smaller than those of the V_O-mediated mechanisms,[14] whereas the formation and rupture of the Magnéli-phase CF in TiO_2, can be either unipolar[9,10] or bipolar,[11,12] depending on the detailed operation method and sample conditions. Therefore, combining these two mechanisms in a single RS material system can be an important research topic for both the mechanistic study and applications. Especially, the exploration of multilevel switching in such a system can be a very important task because many reported multilevel data in a certain RS system usually rely on the degree of a single RS mechanism, which is vulnerable to the large variation during the repeated switching operations.[15,16] The reports on the ECM-type memory cell adopt the various matrix layer, from typical superionic electrolytes such as Cu_2S,[5] which actively participates the RS mechanism, to well-known insulators such as SiO_2[17] and Ta_2O_5,[18] which serves as just a passive matrix for the cation migration and not actively involving the RS itself. In contrast, TiO_2 is a well-known RS material where the fluent electrogeneration of V_O and its percolating path formation are repeatedly reported.[9,12,19]

In this work, therefore, the combined effects of the contributions from the ECM-type Cu-CF and V_O-related RS mechanisms were examined. Due to the simultaneous presence of the two mechanisms in one material system, stable three-level switching can be achieved. The origins of such three-level switching were elucidated through combined analysis using the physicochemical characterizations and electrical conduction properties at each resistance state.

2. EXPERIMENTAL SECTION

TiO_x (200 nm) thin films were simultaneously deposited on 100-nm Cu/5-nm Ti/Si and 100-nm Al/Si substrates via DC magnetron

Received: August 20, 2013
Accepted: October 7, 2013
Published: October 7, 2013

 © 2013 American Chemical Society

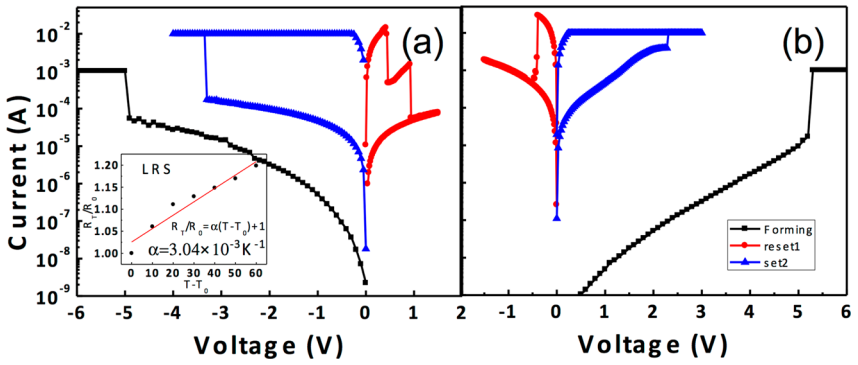

Figure 1. The $I-V$ curves of the (a) AT and (b) CT samples. The black square, red circle, and blue triangle symbols indicate the forming, reset, and set processes, respectively. The inset figure in a shows the variation in the relative resistance as a function of $(T - T_0)$ of LRS.

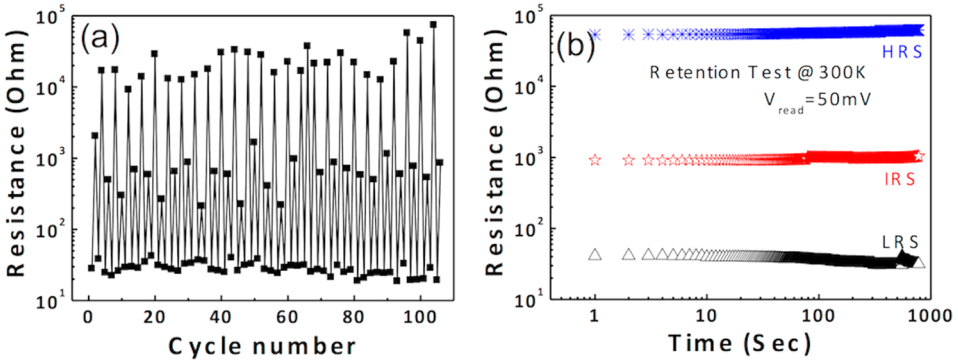

Figure 2. (a) Endurance measurement results of the three resistance levels, where the bias sequence of voltage application was 0 → 0.7 → 0 (achieving IRS) → −5 → 0 (achieving LRS) → 2 → 0 (achieving HRS) → −5 V (achieving LRS again). (b) Retention measurement results of the three resistance levels at room temperature.

sputtering at room temperature, using a 99.995% Ti target and O_2/Ar sputtering gas (1 Pa total pressure, 5% O_2), where all the metal films were electron-beam evaporated. For the measurement of the electrical properties of the TiO_x films, 100-nm-thick top Al and Cu electrodes, respectively, were deposited on TiO_x/Cu and TiO_x/Al via electron beam evaporation, through a metal shadow mask (200 μm hole diameter). The current−voltage (I−V) characteristics of Al/TiO_x/Cu, where Al was the top electrode (TE), called sample AT, and Cu/TiO_x/Al, where Cu was the TE, called sample CT, were measured using an Agilent B1500A semiconductor parameter analyzer at room temperature, unless otherwise stated. All the voltages were applied on the TE while the BE was grounded. The chemical composition and possible diffusion of metal ions into the dielectric layer were examined via depth profiling with an Auger electron spectroscopy (AES, Perkin-Elmer Model 660), and the crystallinity of the TiO_x was examined using an X-ray diffraction (PANalytical, X'pert Pro MPD) in the $\theta-2\theta$ mode. The TiO_x film was weakly crystallized into the anatase phase (data not shown).

3. RESULTS AND DISCUSSION

The resistances of both the pristine AT and CT samples were very high, as indicated by the black square symbols in Figures 1a and 1b, which are the switching $I-V$ curves of the AT and CT samples, respectively. For the AT and CT samples, electroforming was performed using negative and positive bias polarities (1 mA compliance current (I_{cc})), and the typical electroforming voltages were −4 to approcimately −5 and 5−6 V, respectively. When the electroforming of the AT and CT samples were attempted with positive and negative voltages, respectively, the samples also showed electroforming, but the subsequent set (switching from the high-resistance state (HRS) to the low-resistance state (LRS)) and reset (switching from LRS to HRS) operations became unstable, and after only several switching cycles, the samples failed to further switch. Therefore, in this report, the electroforming and subsequent RS operations were accomplished by the sequence of bias applications, as shown in Figure 1. After the electroforming, each sample was electrically swept into the opposite bias region to reset the sample, which was well achieved, as shown by the red circle symbols in Figure 1. The subsequent set was also well achieved by the $I-V$ sweep with the same bias polarity as the electroforming (blue triangle symbol; I_{cc} = 10 mA), with an absolute smaller set voltage (V_{set}) compared with the electroforming voltage. The sample CT shows a typical reset-and-set behavior of the ECM cell, where the formation and rupture of the Cu filament are responsible for the RS behavior, as discussed in detail below. The sample AT, however, shows a clearly distinctive reset curve, as shown in Figure 1a, where a two-step decrease in current at ∼0.5 V (V_{reset}^1) and ∼1 V (V_{reset}^2), respectively, were observed, which is not the case for sample CT. Therefore, sample AT has an intermediate resistance state (IRS) in addition to the usual HRS and LRS.

Such two-step reset was confirmed by $I-V$ sweeps over 100 times, as shown in Figure 2a, which shows the resistance values of HRS, IRS, and LRS, read out at +0.5 V, of the sample AT, as a function of the I−V switching cycle number. Here, the bias sequence of voltage application was 0 → 0.7 → 0 (achieving IRS) → −5 → 0 (achieving LRS) → 2 → 0 (achieving HRS) → −5 V (achieving LRS again). This data set elucidates that the two-step reset in this sample was highly reproducible. Figure 2b shows the retention data of the three states at room temperature up to 1000 s, suggesting that the clearly distinguished states are stable.

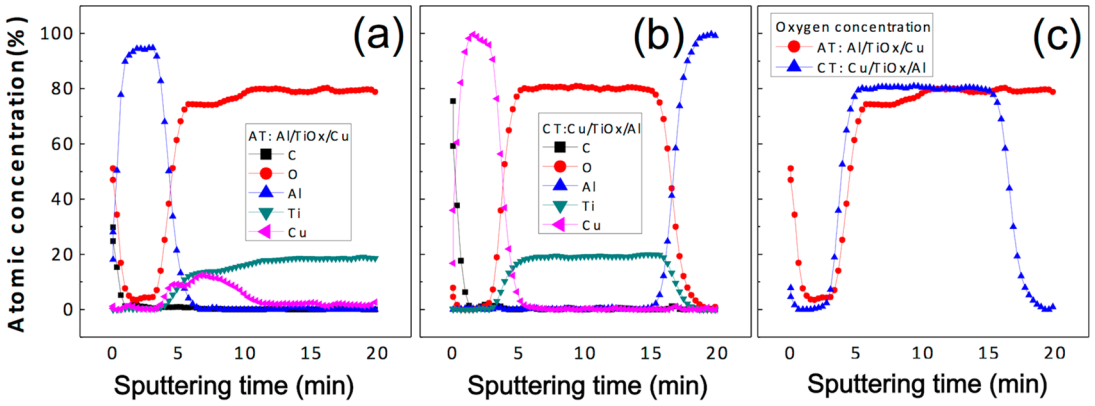

Figure 3. Depth profile results of AES of electroformed sample (a) Al/TiO_x/Cu (sputtering rate 12.2 nm/min for SiO_2) and (b) Cu/TiO_x/Al (sputtering rate: 20.1 nm/min for SiO_2). (c) Oxygen concentration comparison of AT and CT samples. Another AES result of TiO_x/Cu sample (no Al TE) showed abrupt TiO_x/Cu interface as TiO_x/Al interface in (b) (data not shown).

To identify the reasons for obtaining the two-step reset process in sample AT, the temperature-dependent electrical-conduction properties of the three states were examined. The inset of Figure 1a shows the relative resistance variation with respect to the value at room temperature (R_T/R_o) as a function of the temperature difference (T − 300 K) of LRS. Although not shown here, the log I–log V curve of LRS showed a slope of 1, suggesting Ohmic conduction. The data in the inset was fitted according to the general temperature dependency of metal, $R_T/R_o = \alpha(T - T_o) + 1$, where α is the temperature coefficient of resistance, which was estimated to be 3.0×10^{-3} $K^{-1}$from the best-linear-fitting of the data (red line in inset), and T_o = 300 K. This value of α is similar to that of nanoscale Cu,[20−22] suggesting that LRS is achieved by the formation of a Cu conducting filament (Cu-CF) in TiO_x. This must be a reasonable consequence of the sample configuration and bias application scheme; with the Al TE being negatively biased, the Cu^+ ions dissolved from Cu BE into the TiO_x layer electro-migrated onto the interface between Al and TiO_x and were reduced there, forming the Cu-CF seed. As the bias was maintained in the negative region, the Cu-CF grew into Cu BE and finally connected the two electrodes to set the sample. This was further confirmed by the experiment, using the two serially connected TEs to be discussed later. This simple ECM-type model, however, cannot explain the two-step reset behavior in sample AT. Therefore, the following were considered.

Panels a and b in Figure 3 show the AES depth profile results of the electroformed samples AT and CT, respectively. Here, the different sputtering etching rate of 12.2 nm/min and 20.1 nm/min for SiO_2 were used for AT sample and CT sample, respectively, to examine more carefully the oxygen distribution in sample AT. It can be understood from Figure 3c, which shows only the oxygen profiles from the two depth profiles, that the TiO_x at the interface with Al TE certainly shows a relatively low oxygen concentration with a diffused oxygen profile into the Al layer near TiO_x. This is due to the much higher oxidation potential of Al[23] (−527.23 kJ/mol oxygen atomat 300 K) compared with that of TiO_2[23] (−441.46 kJ/mol oxygen atomat 300 K). In contrast, Figure 3b proves that the TiO_x layer in sample CT does not show such obvious decrease in oxygen content near Al BE, which is due to the sufficient supply of oxygen atoms during the sputtering process of TiO_x on Al BE. This cannot be expected for sample AT because the Al layer was formed in a high vacuum condition on the already-deposited TiO_x layer. Therefore, a higher V_O concentration was induced at the Al TE interface for sample AT. Such a high V_O concentration could not have been induced at the Cu TE interface for sample CT because the oxide formation energy of Cu[23] (−128.12 kJ/mol oxygen atomat 300 K) was smaller than that of Ti. Therefore, it can be understood that the TiO_x in sample AT may have induced a conduction channel composed of V_O, in addition to Cu-CF, when Al TE was negatively biased. It is also noted that, as in Figure 3a, the sample AT has a non-negligible concentration of Cu (2−4 at %) in TiO_x region and rather high Cu concentration (~10%) near the Al TE interface, which further confirms the Cu-CF formation in this sample. Kim et al.[24]reported that the CF composed of V_O in TiO_2 was nucleated at the cathode interface (Al in this case) and grew into the anode (Cu in this case), which must have been enhanced by the high V_O concentration at the interface with Al TE. Therefore, the IRS is believed to have been contributed by the remaining V_O-CF while the Cu-CF was already ruptured under the positive bias condition.

It should be noted that the formation of V_O-CF has a relatively low probability once the Cu-CFs are formed under the negative bias because much of the current flows along the Cu-CF. Localized current flow at local spots that are not coincident with the locations of the Cu-CFs is necessary to induce the V_O-CF because V_O-CF formation is driven by the Joule-heating-effect-assisted electro-migration of oxygen ions.[25] Therefore, only sample AT had a high probability of forming V_O-CF even after (or simultaneously with) the formation of the Cu-CFs, because of the high V_O concentration near Al TE, which largely enhanced the electron injection into the TiO_x layer and the consequent Joule heating effect. This cannot be expected from sample CT because the Al BE interface could not bear a high V_O concentration. As such, electron injection from Al to the TiO_x region at the regions other than the Cu-CF region must be suppressed, and V_O-CF formation was thus also suppressed. Therefore, it was expected that only Cu-CF would be formed in sample CT, whereas the V_O-CF is considered to have coexisted with Cu-CF in sample AT.

The mechanism mentioned above was further confirmed by the following experiments. Two TEs in sample AT were taken and biased, as shown in the inset schematic figures in panels a and b in Figure 4. In a, one Al TE (TE A) was pulse-biased with +8 V for 1 ms while the other Al TE (TE B) was grounded and Cu BE was floated. In b, the same was performed, except for the negative pulse voltage on TE A. When the pulse was turned off, the resistances between TE A and Cu BE and between TE

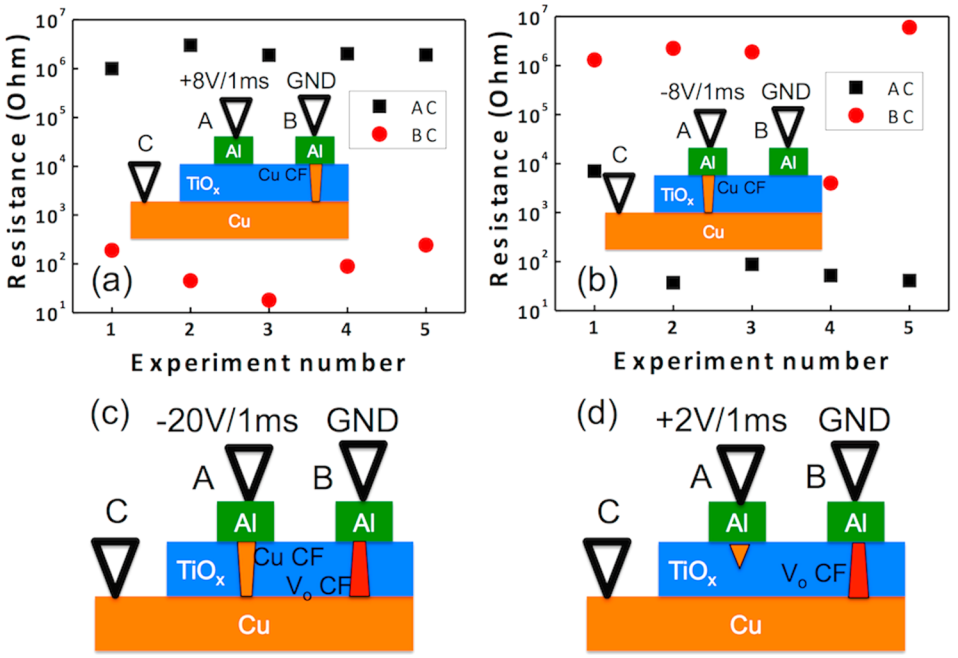

Figure 4. Measured resistance values of AC and BC as a function of the repeat times, under (a) positive pulse to TE A and (b) negative pulse to TE A while both TE Bs were grounded. The insets in a and b show the schemes where the two TEs in sample AT were taken and biased. (c) Formation of Cu-CF and V_o-CF in AC and BC, respectively, after applying a −20 V/1 ms pulse voltage to TE A while TE B was grounded. (d) After reset by applying +2 V, 1 ms to TE A while TE B was grounded. The resistances of AC and BC were monitored at 50 mV.

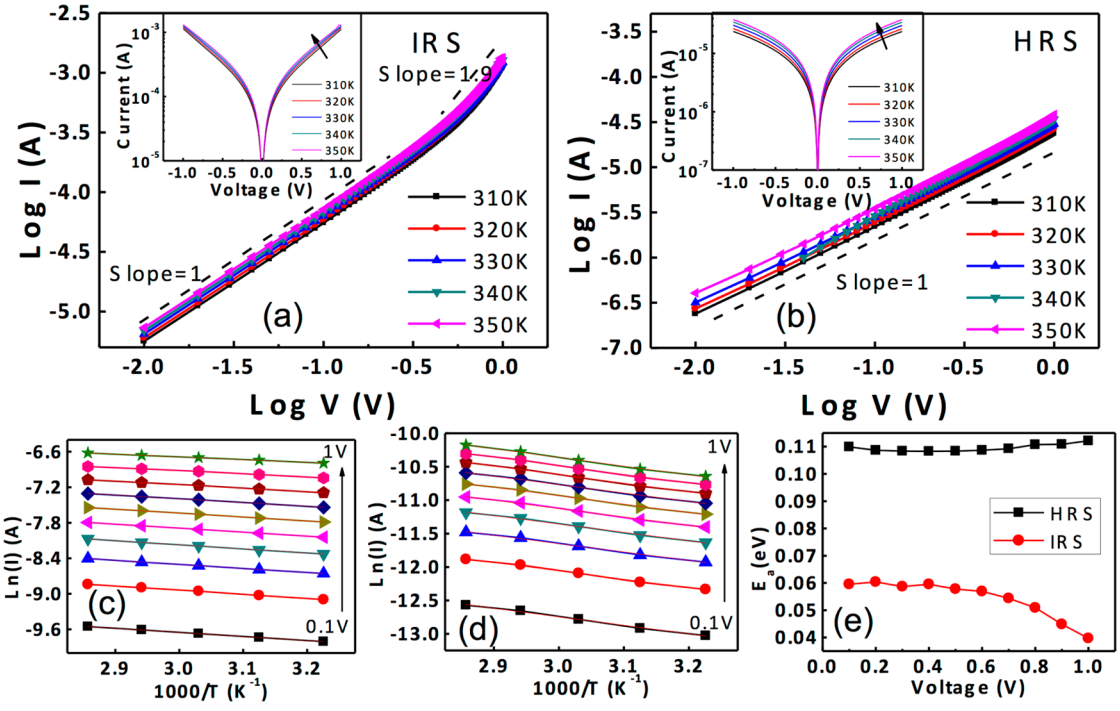

Figure 5. Log *I*–log *V* curves of (a) IRS and (b) HRS at measurement temperatures ranging from 310 to 350 K. The insets in a and b show that the *I*–*V* curves of IRS and HRS increase with increasing temperature. Ln *I* vs 1000/*T* curves of (c) IRS and (d) HRS at the given V. (e) Variations in the activation energy calculated from the slopes of the best-linear-fitted graphs of c and d as a function of *V*.

B and Cu BE were estimated at a voltage of 50 mV. This experiment was repeated five times, and the results are summarized in panels a and b in Figure 4. Under these pulse bias conditions, the TE, which was cathodic-biased (TE B in a and TE A in b) during the pulse application, had low resistance, meaning that the Cu-CFs were formed only in those cells. This was a natural consequence of the different potential distributions for the Cu-CF formation for TE A and TE B. The anodic-biased cells could not have had Cu-CF formation because the Al electrode had a higher electric potential than the Cu electrode.

Decreasing the pulse voltage to −20 V for the same duration, however, as shown in Figure 4c, turned on both the TE A and TE B cells. This can be interpreted to mean that the anodic

biased cell, TE B, as shown in Figure 4c, came to have V_O-CF, whereas the TE A cell had Cu-CF. This could not have exactly reproduced the sequential (or simultaneous) formation of Cu-CF and V_O-CF, however, in Figures 1a and 2a because the V_O-CF in Figure 4c must nucleate from the Cu BE interface and must grow onto the Al TE interface, but it grew in the opposite direction in Figure 1a. The following reset experiments of the serially connected cells clearly demonstrated, however, that Cu-CF was preferably ruptured before V_O-CF. Figure 4d shows the schematic diagram of the same serially connected cell as that in Figure 4c after reset by applying +2 V, 1 ms to TE A while TE B was grounded, and the resistances between TE A and Cu BE and between TE B and Cu BE were monitored at 50 mV. Then the serially connected sample was set again using −20 V at TE A, as was done in Figure 4c, and was subsequently reset, after which the resistances of the TE A and TE B cells were measured. This was repeated 54 times, and 46 results showed that TE A had HRS while TE B maintained LRS after the series reset. This is a strong indication that Cu-CF had a lower reset voltage than V_O-CF, which is also in agreement with the other ECM and valence chance memory (VCM) cells, where the ECM cells generally showed lower switching voltages than the VCM cells.[14] It is highly probable that very thin AlO_x layer is formed at the Al/TiO_x interface. However, it is believed that the thickness of this layer should not be thick enough to interfere with the electroforming and subsequent RS properties due to the limited supply of oxygen from TiO_x layer. The well-explained electrical RS properties by using the suggested Cu-CF and Vo-CF model indirectly prove this argument. In addition, the local spots where the CFs formed may be devoid of such thin AlO_x layer by electrical breakdown during the switching.

Finally, the electrical-conduction mechanisms of IRS and HRS were examined to further elucidate the switching mechanism mediated by the remaining V_O-CFs after the first reset at V_{reset}^1 of sample AT. The inset figures in panels a and b in Figure 5 show the $I-V$ curves measured at temperatures ranging from 310 to 350 K after the sample's transformation into IRS and HRS, respectively, and the main figures show the log I−log V plot of the same data set in the positive (0 → +1 V) voltage region. Both states showed an increase in current with increasing temperature, where the increase was more dominant for HRS. The log I−log V plot of IRS shows a slope of 1 at voltages <0.4 V, and 1.9 at voltages >0.6 V, suggesting that the electrical conduction was due to the trap-filled space-charge-limited conduction.[11] The data were plotted again in Arrehnius form, as shown in Figure 5c, and the activation energy (E_a) at each applied voltage was calculated from the best-linear-fittings of the data, which are summarized in Figure 5e (red circle symbol). The E_a values are quite low and constant (~0.06 eV) at voltages $\lesssim$0.6 V, which coincides with the report of Kim et al.,[11] where the electronic RS mechanism involving the trapping and detrapping of electrons at the V_O channel in TiO_2 was elucidated. At the voltages >0.6 V, E_a slightly decreases with increasing voltage. This is due to the fact that the traps with higher depth (or E_a) were already filled with electrons and other traps with slightly shallower depth are now responding to the voltage. The log I−log V curves of HRS in Figure 5b show a slope of 1 in the entire voltage region (up to 1 V), with slightly higher E_a values of ~0.11 eV, as shown in panels d and e in Figure 5 (black square symbol). This well coincides with the electron hopping model for the trapped electrons with electron-detrapped oxygen vacancies.[11] Attempts to fit the data with other conduction models, such as Schottky emission, Poole-Frenkel emission, and Fowler-Nordheim tunneling, failed. Therefore, it can be concluded that IRS and HRS are characterized by electron-trapped and electron-detrapped V_O channels, where the transition between the two occurs electronically.

4. CONCLUSIONS

In summary, the two-step reset behaviors in the RS properties in the Al TE/TiO_x/Cu BE sample were studied in detail. During the electroforming and set step, Cu-CFs and V_O-CFs were simultaneously (or primarily Cu-CFs) formed when Al TE was negatively biased. During the subsequent reset step in the positive-bias region to Al TE, the Cu-CFs ruptured first at ~0.5 V and then formed an intermediate resistance state, where the electrical conduction was dominated by the trap-filled V_O-CFs, which revealed the space-charge-limited conduction. With a further increase in the reset voltage up to ~1 V, the electrons were detrapped from the V_O channel, and sample switches to HRS and electron transport occurred through the hopping mechanism. This study revealed that the nominal "electrolyte" in the ECM cell, which is supposed to be an inactive media for ion transport, can play an active role in the RS of the ECM-type RS memory.

AUTHOR INFORMATION

Corresponding Authors

*E-mail: cheolsh@snu.ac.kr.

*E-mail: jinshi58@163.com.

Notes

The authors declare no competing financial interest.

ACKNOWLEDGMENTS

This work was supported by the National Natural Science Foundation of China (Grants 61274113 and 11204212), the Program for New-Century Excellent Talents in University, China (Grant NCET-11-1064), Tianjin Natural Science Foundation, China (Grants 10SYSYJC27700, 13JCYBJC15700, and 10ZCKFGX01200), and Tianjin Science and Technology Developmental Funds of Universities and Colleges, China (Grant 20100703). C.S.H. acknowledges the support of the Global Research Laboratory Program (2012040157) through the National Research Foundation (NRF) of Korea.

REFERENCES

(1) Waser, R.; Aono, M. *Nat. Mater.* **2007**, *6*, 833−840.

(2) Waser, R.; Dittmann, R.; Staikov, G.; Szot, K. *Adv. Mater.* **2009**, *21*, 2632−2663.

(3) Kim, K. M.; Jeong, D. S.; Hwang, C. S. *Nanotechnology* **2011**, *22*, 254002.

(4) Yang, J. J.; Inoue, I. H.; Mikolajick, T.; Hwang, C. S. *MRS Bull.* **2012**, *37*, 131−137.

(5) Nayak, A.; Ohno, T.; Tsuruoka, T.; Terabe, K.; Hasegawa, T.; Gimzewski, J. K.; Aono, M. *Adv. Funct. Mater.* **2012**, *22*, 3606−3613.

(6) Kozicki, M. N.; Balakrishnan, M.; Gopalan, C.; Ratnakumar, C.; Mitkova, M. *Non-Volatile Memory Technology Symposium*; Dallas, TX, Nov 7−10, 2005 ; IEEE: Piscataway, NJ, **2005**,; pp 83−−89.

(7) Liu, Q.; Sun, J.; Lv, H.; Long, S.; Yin, K.; Wan, N.; Li, Y.; Sun, L.; Liu, M. *Adv. Mater.* **2012**, *24*, 1844−1849.

(8) Gao, S.; Song, C.; Chen, C.; Zeng, F.; Pan, F. *J. Phys. Chem. C.* **2012**, *116*, 17955−17959.

(9) Choi, B. J.; Jeong, D. S.; Kim, S. K.; Rohde, C.; Choi, S.; Oh, J. H.; Kim, H. J.; Hwang, C. S.; Szot, K.; Waser, R.; Reichenberg, B.; Tiedke, S. *J. Appl. Phys.* **2005**, *98*, 033715.

(10) Kwon, D.-H.; Kim, K. M.; Jang, J. H.; Jeon, J. M.; Lee, M. H.; Kim, G. H.; Li, X.-S.; Park, G.-S.; Lee, B.; Han, S.; Kim, M.; Hwang, C. S. *Nat. Nanotechnol.* **2010**, *5*, 148−153.
(11) Kim, K. M.; Choi, B. J.; Lee, M. H.; Kim, G. H.; Song, S. J.; Seok, J. Y.; Yoon, J. H.; Han, S.; Hwang, C. S. *Nanotechnology* **2011**, *22*, 254010.
(12) Yoon, K. J.; Lee, M. H.; Kim, G. H.; Song, S. J.; Seok, J. Y.; Han, S.; Yoon, J. H.; Kim, K. M.; Hwang, C. S. *Nanotechnology* **2012**, *23*, 185202.
(13) Yu, L. E.; Kim, S.; Ryu, M. K.; Choi, S. Y.; Choi, Y. K. *IEEE Electron Device Lett.* **2008**, *29*, 331−333.
(14) Valov, I.; Waser, R. *Adv. Mater.* **2012**, *25*, 162−164.
(15) Park, J.; Biju, K. P.; Jung, S.; Lee, W.; Lee, J.; Kim, S.; Park, S.; Shin, J.; Hwang, H. *IEEE Electron Device Lett.* **2010**, *32*, 476−478.
(16) Zhang, Y.; Wu, H.; Bai, Y.; Chen, A.; Yu, Z.; Zhang, J.; Qian, H. *Appl. Phys. Lett.* **2013**, *102*, 233502.
(17) Schindler, C.; Weides, M.; Kozicki, M. N.; Waser, R. *Appl. Phys. Lett.* **2008**, *92*, 122910.
(18) Valov, I.; Kozicki, M. N. *J. Phys. D: Appl. Phys.* **2013**, *46*, 074005.
(19) Rohde, C.; Choi, B. J.; Jeong, D. S.; Choi, S.; Zhao, J.-S.; Hwang, C. S. *Appl. Phys. Lett.* **2005**, *86*, 262907.
(20) Guan, W.; Liu, M.; Long, S.; Liu, Q.; Wang, W. *Appl. Phys. Lett.* **2008**, *93*, 223506.
(21) Zhuge, F.; Peng, S.; He, C.; Zhu, X.; Chen, X.; Liu, Y.; Li, R.-W. *Nanotechnology* **2011**, *22*, 275204.
(22) Liu, Q.; Jun, S.; Lv, H.; Long, S.; Li, L.; Yin, K.; Wan, N.; Li, Y.; Sun, L.; Liu, M. *Adv. Mater.* **2012**, *25*, 165−167.
(23) Barin, I.; Platzki, G. *Thermochemical Data of Pure Substances*, 3rd ed.; Sora, K., Gardiner. J., Eds; VCH: Weinheim, Germany, 1995.
(24) Kim, K. M.; Choi, B. J.; Shin, Y. C.; Choi, S.; Hwang, C. S. *Appl. Phys. Lett.* **2007**, *91*, 012907.
(25) Kim, K. M.; Hwang, C. S. *Appl. Phys. Lett.* **2009**, *94*, 122109.